Providence, RI
NOISE-CON 2016
2016 June 13–15

Hybrid Feedforward-Feedback Noise Control using Virtual Sensors

Jacob Bean, *Virginia Polytechnic Institute and State University*
Chris Fuller, *Virginia Polytechnic Institute and State University*
Noah Schiller, *NASA Langley Research Center*

ABSTRACT

Several approaches to active noise control using virtual sensors are evaluated for eventual use in an active headrest. Specifically, adaptive feedforward, feedback, and hybrid control structures are compared. Each controller incorporates the traditional filtered-x least mean squares algorithm. The feedback controller is arranged in an internal model configuration to draw comparisons with standard feedforward control theory results. Simulation and experimental results are presented that illustrate each controllers ability to minimize the pressure at both physical and virtual microphone locations. The remote microphone technique is used to obtain pressure estimates at the virtual locations. It is shown that a hybrid controller offers performance benefits over the traditional feedforward and feedback controllers. Stability issues associated with feedback and hybrid controllers are also addressed. Experimental results show that 15-20 dB reduction in broadband disturbances can be achieved by minimizing the measured pressure, whereas 10-15 dB reduction is obtained when minimizing the estimated pressure at a virtual location.

1 Introduction

The idea of active noise control (ANC), proposed by Paul Lueg [1] in 1936, exploits the principle of acoustic superposition to cancel disturbances in a system through the introduction of secondary sources. These secondary sources, typically loudspeakers in ANC, are driven by an electronic controller such that disturbances to the system under control are attenuated. Due to a lack of technology at the time, this idea did not become feasible until several decades later. Numerous advances in digital signal processing technology and adaptive filtering theory have given rise to the study and development of many practical ANC systems [2]. ANC systems grant benefits over traditional passive control strategies as they are non-intrusive, portable, cheap, and offer significant performance advantages at low frequencies [3,4].

The majority of ANC algorithms operate adaptively, although a variety of fixed control approaches based on optimal filtering, LQG theory, and loop shaping have been proposed [5,6,7]. Adaptive controllers enjoy the flexibility of being capable of adapting to time-varying plants and non-stationary disturbances. Most adaptive ANC algorithms are based on the least mean squares (LMS) algorithm pioneered in [8]. The most common of these is the filtered-x LMS algorithm. The filtered-x LMS algorithm accounts for the presence of the secondary path (the control to error path) by pre-filtering the reference signal with a model of the secondary path [8,9]. Due to it's simplicity and ease of implementation, this algorithm is widely used in active noise and vibration control applications [9].

This paper investigates the behavior of three different adaptive control approaches using a virtual error sensor: feedforward control, feedback control, and hybrid control. The purpose of this analysis is to evaluate the feasibility of implementation of these control algorithms on an active headrest. In the literature, performance studies of active headrests have employed feedforward [10] and feedback controllers [11,12,13]. Active headrests that use adaptive feedback controllers are in general capable of attenuating only tonal disturbances, while those that employ feedforward controllers attenuate disturbances that are correlated with a reference signal [2,3,4]. It seems logical that an active headrest employing a hybrid controller [14] (a combination of feedforward and feedback) may result in improved broadband performance. It will be shown that in scenarios where the disturbance contains tonal components that are not correlated with the reference signal, the hybrid controller offers considerable performance advantages over a feedforward or feedback system alone. In each of these cases, the controller minimizes the sound pressure at the location of a physical microphone. In the case of an active headrest, it is desirable to locate the quiet zone at an occupant's eardrums as opposed to the physical microphone locations. The remote microphone technique [15] will be used in this study to provide pressure estimates at a virtual location.

The rest of the paper is organized as follows. In Section 2, the adaptive control algorithm will be derived and it's incorporation into feedforward, feedback, and hybrid control will be introduced. Section 3 provides computer simulation results of the three control structures. Experimental results are then presented in Section 4.

2 Control Approach

In this section, the filtered-*x* LMS algorithm will be derived and it's incorporation into adaptive feedforward, feedback, and hybrid control structures is introduced. Performance characteristics of the three control structures will also be discussed.

A Adaptive Feedforward Control

The following derivation closely follows the discussion in [9]. Consider the block diagram of Figure 1. The upstream reference signal is denoted $x(n)$. If the adaptive control filter, $A(z)$, and the secondary path model, $G_{cp}(z)$, are modeled as finite impulse response (FIR) filters, the error signal is

$$e(n) = d(n) + \sum_{j=0}^{J-1} g_{cp,j} \sum_{i=0}^{I-1} a_i(n-j)x(n-i-j), \tag{1}$$

where $g_{cp,j}$ is the j^{th} coefficient of the impulse response of the secondary path and a_i is the i^{th} control filter coefficient. Under the assumption of slow control filter adaption, the controller and plant may be transposed. The filtered-*x* LMS algorithm accounts for the presence of the secondary path by pre-filtering the reference signal with a secondary path model, $\hat{G}_{cp}(z)$. Let the filtered reference signal, $\hat{x}(n)$, be defined

$$\hat{x}(n) = \sum_{j=0}^{J-1} \hat{g}_{cp,j} x(n-j), \tag{2}$$

where $\hat{g}_{cp,j}$ is the j^{th} coefficient of the impulse response of the secondary path model. The error signal may then be written as

$$e(n) = d(n) + \sum_{i=0}^{I-1} a_i \hat{x}(n-i). \tag{3}$$

Or in vector notation,

$$e(n) = d(n) + \mathbf{a}^T(n)\hat{\mathbf{x}}(n), \tag{4}$$

where

$$\mathbf{a}(n) = [a_0,\ a_1,\ \cdots,\ a_{I-1}]^T, \tag{5}$$

$$\hat{\mathbf{x}}(n) = [\hat{x}(n),\ \hat{x}(n-1),\ \cdots,\ \hat{x}(n-I+1)]^T. \tag{6}$$

The cost function to be minimized is the mean square error (MSE),

$$J = E\left[e^2(n)\right]. \tag{7}$$

The fundamental idea of the gradient descent method is to compute the gradient of the cost function with respect to the control filter coefficients and adapt the coefficients in such a way that they approach values that minimize Eq. 7, *i.e.*

$$\mathbf{a}(n+1) = \mathbf{a}(n) + \alpha\left(-\nabla J\right), \tag{8}$$

where α is the learning rate of the controller. The optimal learning rate is determined by the eigenvalues of the autocorrelation matrix of the filtered reference signal [9]. With exact knowledge of the gradient, the filter coefficients could be adapted to their exact H_2 optimal values, such as is the case in the recursive least squares (RLS) algorithm [8]. Because this controller is adaptive, exact knowledge of the gradient is unknown and an instantaneous stochastic estimate must be used. Expanding Eq. 7 gives

$$J(n) = E\left[d^2(n)\right] + 2\mathbf{a}^T E\left[d(n)\hat{\mathbf{x}}(n)\right] + \mathbf{a}^T E\left[\hat{\mathbf{x}}^T(n)\hat{\mathbf{x}}(n)\right]\mathbf{a}, \tag{9}$$

where the dependence of the controller filter on sample number has been suppressed because it is assumed to be adapting slowly compared to the timescales of the plant dynamics. Clearly, the cost function is quadratic in the control filter coefficients. Therefore a global minimum is guaranteed to exist. Taking the gradient results in

$$\nabla J(n) = 2e(n)\hat{\mathbf{x}}(n). \tag{10}$$

This leads to the control filter update equation

$$\mathbf{a}(n+1) = \mathbf{a}(n) - \alpha\hat{\mathbf{x}}(n)e(n). \tag{11}$$

The gradient defined by Eq. 10 is essentially an estimate of the cross correlation between the error and filtered reference signals. Thus the convergence of the algorithm is highly sensitive to this estimate. This illustrates the importance of identifying an accurate plant model to pre-filter the reference signal. It is apparent that only disturbances that are correlated with the reference signal are capable of being attenuated by the feedforward controller. This algorithm has been shown to converge for plant model estimates within $\pm 90^\circ$ of the true plant response [16].

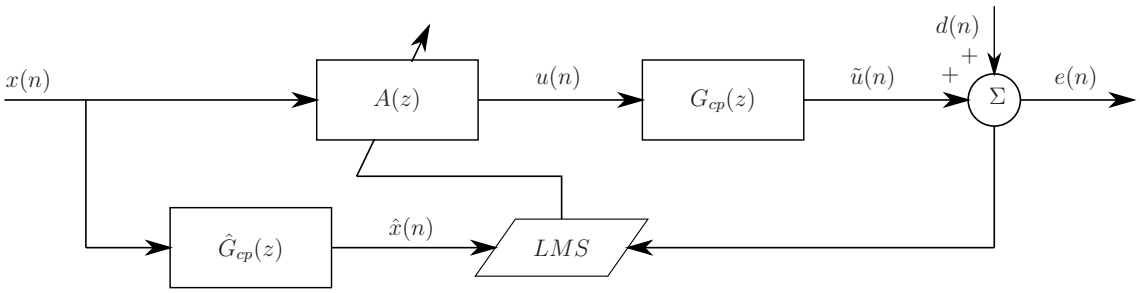

Figure 1: Block diagram of a feedforward controller using the F*x*LMS algorithm.

B Adaptive Feedback Control

In contrast to feedforward control, feedback structures generate a control signal based only upon the output of the error sensor. This results in a more compact control system but may suffer in performance due to a lack of time advanced knowledge on the disturbance. A common approach to feedback ANC is to use internal model control (IMC) [17] to transform the problem into an equivalent feedforward one. This is accomplished by including a model of the plant in the feedback loop that is used to internally synthesize a reference signal that can be used in a feedforward configuration. Figure 2 shows a block diagram of a feedback controller with an internal plant model. The error signal is the summation of the disturbance and the output of the controller after being filtered through the secondary path. Using an internal plant model, the primary noise, $d(n)$, can be estimated by subtracting the control signal filtered through the plant model from the measured error signal. This signal may then be used as a reference signal in a feedforward sense. The internally synthesized reference signal is

$$z(n) = e(n) - \hat{G}_{cp}(z)v(n). \tag{12}$$

This signal may be thought of as the true reference signal, $x(n)$, in the feedforward configuration. The control filter is then updated according to

$$\mathbf{c}(n+1) = \mathbf{c}(n) - \alpha\hat{\mathbf{z}}(n)e(n), \tag{13}$$

where

$$\hat{z}(n) = \sum_{j=0}^{J-1} \hat{g}_{cp,j} z(n-j), \tag{14}$$

$$\mathbf{c}(n) = [c_0,\ c_1,\ \cdots,\ c_{I-1}]^T, \tag{15}$$

$$\hat{\mathbf{z}}(n) = [\hat{z}(n),\ \hat{z}(n-1),\ \cdots,\ \hat{z}(n-I+1)]^T. \tag{16}$$

The sensitivity function for the IMC configuration of Figure 2 is given by

$$S(z) = \frac{1 + \hat{G}_{cp}(z)C(z)}{1 - \left[G_{cp}(z) - \hat{G}_{cp}(z)\right] C(z)}. \tag{17}$$

It is a well known result that for disturbance rejection in a feedback controller, the sensitivity function must be minimized [9]. This will occur when the loop gain,

$$L(z) = \left[\hat{G}_{cp}(z) - G_{cp}(z)\right] C(z), \tag{18}$$

is small, causing the denominator of Eq. 17 to approach unity. This will occur when the frequency response of the plant model is sufficiently close to that of the true plant. Even when this is the case, large values of control filter coefficients may cause Eq. 18 to approach unity, resulting in a non-quadratic error surface [18].

Insight into the performance of this adaptive IMC controller can be gained by assuming a perfect plant model, *i.e.* $\hat{G}_{cp}(z) = G_{cp}(z)$. Under this assumption the problem is entirely feedforward, with $d(n)$ acting simultaneously as the reference and disturbance signal. This simplification is *only* possible under the assumption of a perfect plant model, because with exact knowledge of the plant there is no need for a feedback path [17]. If it is further assumed that the plant transfer function is a pure delay, the problem reduces to that of the adaptive predictor. Under these conditions, the control filter is acting as an adaptive predictor of the primary noise [3], thus it's performance will depend on the predictability of the primary noise. It follows that the adaptive feedback controller is best suited for the attenuation of narrow-band disturbances. The performance of the adaptive IMC controller is limited by the bandwidth of the disturbance as well as the delay in the plant [9].

More care must be taken when implementing the feedback F*x*LMS controller as opposed to the feedforward controller. While the feedforward F*x*LMS algorithm is inherently stable for slow adaption or fixed controller coefficients, the same cannot be said for the feedback controller. The feedback controller does not obey the conventional $\pm 90^\circ$ convergence requirement as the feedforward controller [19]. This is because the true filter that should be used to pre-filter the reference signal is itself a function of the feedback controller. The $\pm 90^\circ$ convergence criteria was derived assuming that the filter used to pre-filter the reference signal is independent of the control filter. The presence of the feedback loop causes this assumption to be violated. It follows that instabilities may arise due to divergence of the adaptive algorithm as well as the presence of the feedback loop (*i.e.* if the poles of Eq. 17 migrate outside of the unit circle). It is shown in [19] that the proper convergence condition for the feedback controller is

$$\angle \left(\frac{G_{cp}(z)}{\left(1 - \left[G_{cp}(z) - \hat{G}_{cp}(z)\right] W(z)\right)^2} \right) - \angle \left(\frac{\hat{G}_{cp}(z)}{1 - \left[G_{cp}(z) - \hat{G}_{cp}(z)\right] W(z)} \right) < 90^\circ. \quad (19)$$

It should be noted that if a perfect plant model is assumed, this condition reduces to the conventional convergence requirement given by

$$\angle G_{cp}(z) - \angle \hat{G}_{cp}(z) < 90^\circ. \quad (20)$$

C Adaptive Hybrid Control

The feedforward and feedback controllers of Figure 1 and Figure 2 each offer specific performance advantages. The performance of the feedforward controller is highly dependent upon the quality of the reference signal. Thus for satisfactory performance it is necessary that a coherent reference signal be available. In many cases, the reference will not be perfectly correlated with the disturbance. Adaptive feedback control can then be used to attenuate these uncorrelated disturbances. In such scenarios, it is appealing to consider a hybrid control architecture. A hybrid control structure is shown in Figure 3. This structure utilizes the feedforward controller, $A(z)$, to attenuate disturbances that are correlated with the reference while the feedback controller, $C(z)$, attenuates disturbances that are not correlated with the reference signal.

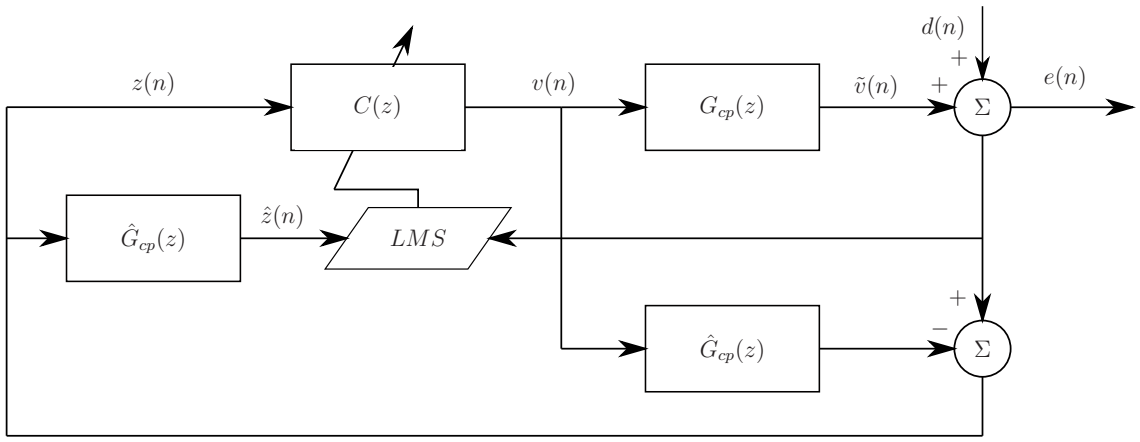

Figure 2: Block diagram of a feedback controller using the F*x*LMS algorithm with internal plant model.

Due to the addition of a feedback loop, new dynamics are introduced that influence the feedforward controller. This can be seen by computing the error signal as a function of the control filters and secondary paths. First note that the reference signal for the feedback controller is

$$z(n) = e(n) - \hat{G}_{cp}(z)\left(A(z)x(n) + C(z)z(n)\right). \tag{21}$$

Solving for $z(n)$ gives

$$z(n) = \frac{1}{1 + \hat{G}_{cp}(z)C(z)}e(n) - \frac{\hat{G}_{cp}(z)A(z)}{1 + \hat{G}_{cp}(z)C(z)}x(n). \tag{22}$$

The error signal is

$$e(n) = d(n) + G_{cp}(z)A(z)x(n) + G_{cp}(z)C(z)z(n). \tag{23}$$

Inserting Eq. 22 into Eq. 23 results in

$$e(n) = \frac{1 + \hat{G}_{cp}(z)C(z)}{1 - \left[G_{cp}(z) - \hat{G}_{cp}(z)\right]C(z)}d(n) + \frac{G_{cp}(z)A(z)}{1 - \left[G_{cp}(z) - \hat{G}_{cp}(z)\right]C(z)}x(n) \tag{24}$$

The update law of the adaptive controller is found by evaluating the gradient of the MSE cost function, Eq. 7, with respect to each control filter. The gradient of the cost function is

$$\nabla J(n) = 2e(n)\left[\nabla e(n)\right], \tag{25}$$

which is linearly dependent on the gradient of the error signal, $e(n)$. The gradient of the error signal with respect to the feedforward control filter is

$$\frac{\partial e(n)}{\partial \mathbf{a}} = \frac{G_{cp}(z)}{\left(1 - \left[G_{cp}(z) - \hat{G}_{cp}(z)\right]C(z)\right)^2}x(n). \tag{26}$$

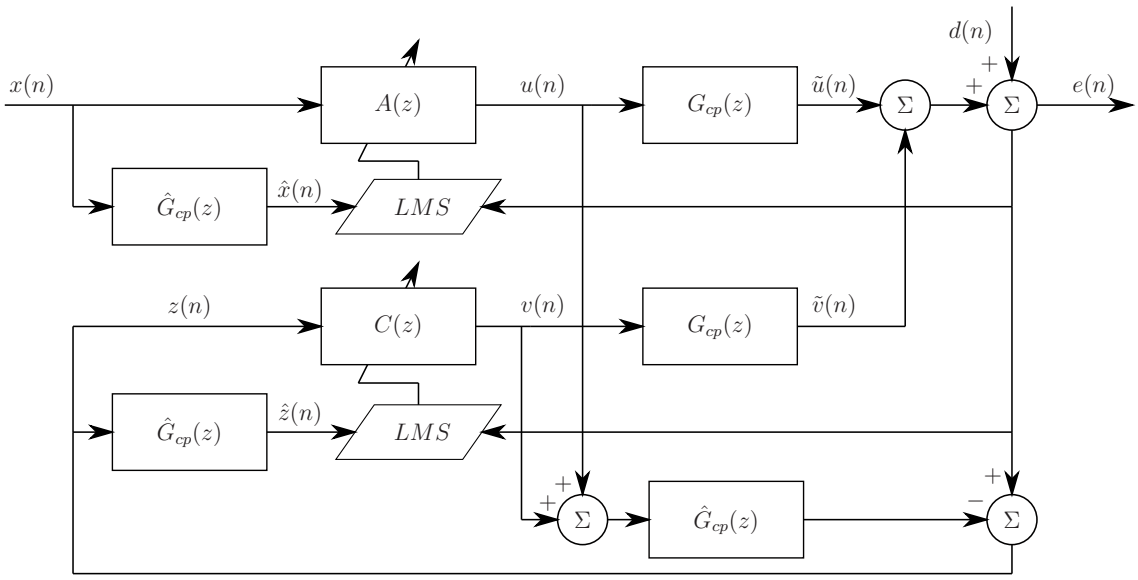

Figure 3: Block diagram of a hybrid feedforward-feedback controller using the F*x*LMS algorithm with internal plant model.

The gradient with respect to the feedback control filter is

$$\frac{\partial e(n)}{\partial \mathbf{c}} = \frac{G_{cp}(z)}{\left(1 - \left[G_{cp}(z) - \hat{G}_{cp}(z)\right] C(z)\right)^2} d(n) + \frac{A(z)G_{cp}(z)\left[G_{cp}(z) - \hat{G}_{cp}(z)\right]}{\left(1 - \left[G_{cp}(z) - \hat{G}_{cp}(z)\right] C(z)\right)^2} x(n). \quad (27)$$

The gradients computed in Eq. 26 and Eq. 27 are impossible to calculate exactly because the true plant response, $G_{cp}(z)$ is unknown. To estimate these gradients, it is common to assume that the plant model is accurate, *i.e.* $\hat{G}_{cp}(z) \approx G_{cp}(z)$. Eq. 26 and Eq. 27 then reduce to

$$\frac{\partial e(n)}{\partial \mathbf{a}} = \hat{G}_{cp}(z)x(n), \quad (28)$$

and

$$\frac{\partial e(n)}{\partial \mathbf{c}} = \hat{G}_{cp}(z)d(n). \quad (29)$$

The estimated plant response has also been substituted into Eq. 28 and Eq. 29. Of course the primary disturbance, $d(n)$, is unknown and must be estimated as described by Eq. 12. The update equations for the hybrid ANC controller are then

$$\mathbf{a}(n+1) = \mathbf{a}(n) - \alpha_1 \hat{\mathbf{x}}(n)e(n), \quad (30)$$

$$\mathbf{c}(n+1) = \mathbf{c}(n) - \alpha_2 \hat{\mathbf{z}}(n)e(n), \quad (31)$$

where the filtered reference signals defined in Eq. 2 and Eq. 14 were used. Each control filter now appears to be learning independently. This is only due to the assumption of a perfect plant model. Both controllers are in reality still coupled. The term $\left[G_{cp}(z) - \hat{G}_{cp}(z)\right] C(z)$ remaining small is critical to the avoidance of algorithm divergence and feedback loop instabilities. It is common in practice to include a leakage term in the update equation of the feedback controller to avoid such instabilities.

D Virtual Sensing

The previous discussions revolve around ANC systems that are designed to minimize the mean square error of the pressure signal at the location of an error sensor. This creates a so called *zone of silence* around the error sensor. The size and shape of these zones are disturbance dependent and may be highly irregular. The size of these zones has been investigated by a number of authors and is found to be roughly $1/10$ of the wavelength of the disturbance. In some cases it may be desirable to reduce noise in areas that are unfit for physical microphones (such as a person's eardrums). Such limitations bring about the idea of virtual sensing. Virtual sensing provides a means of estimating the pressure at a remote, or virtual, location based on known information. In most cases, a physical sensor is used to measure the pressure. This measurement is then used in a virtual sensing algorithm to estimate the pressure at the virtual microphone location.

The virtual sensing algorithm used in the current study is the remote microphone technique (RMT) [15]. This technique, used with the control algorithms discussed herein, involves the preliminary identification of three transfer functions. These include the path from the control to the physical error sensor, $G_{cp}(z)$, the path from the control to the virtual error sensor, $G_{cv}(z)$, and the path from the physical error sensor to the virtual error sensor, $G_{pv}(z)$. To model the last two, physical microphones are temporarily placed at the virtual locations during a preliminary identification stage. These microphones are then removed during operation of the ANC system. For the purpose of the experiment, microphones are left in the virtual locations to monitor control performance. In the following, subscripts p and v refer to physical and virtual locations, respectively. The hat superscript denotes estimated quantities. The algorithm will be derived in the context of a feedforward controller, but it may be easily extended to the feedback and hybrid structures.

The first step in this algorithm is to estimate the signal at the physical error sensor due solely to the primary disturbance. This is given by

$$\hat{d}_p(n) = e_p(n) - \hat{G}_{cp}(z)u(n), \tag{32}$$

If each of the identified paths are modeled as FIR filters, this becomes

$$\hat{d}_p(n) = e_p(n) - \sum_{i=0}^{I-1} a_i \hat{x}(n-i), \tag{33}$$

where $\hat{x}(n)$ is the filtered reference signal defined in Eq. 2. The estimate of the primary disturbance at the virtual sensor is given by filtering the estimated disturbance at the physical microphone through the physical error sensor to virtual error sensor path. This is written

$$\hat{d}_v(n) = \hat{G}_{pv}(z)\hat{d}_p(n), \tag{34}$$

or using the FIR notation,

$$\hat{d}_v(n) = \sum_{j=0}^{J-1} \hat{g}_{pv_j} \hat{d}_p(n-j). \tag{35}$$

Now, the virtual error signal to be minimized can be written

$$\hat{e}_v(n) = \hat{G}_{pv}(z)\hat{d}_p(n) + \hat{G}_{cv}(z)u(n). \tag{36}$$

or equivalently

$$\hat{e}_v(n) = \sum_{j=0}^{J-1} \hat{g}_{pv_j} \hat{d}_p(n-j) + \sum_{i=0}^{I-1} a_i \hat{x}_v(n-i). \tag{37}$$

Here, $\hat{x}_v(n)$ is the reference signal filtered through the control to virtual sensor path,

$$\hat{x}_v(n) = \sum_{j=0}^{J-1} \hat{g}_{cv_j} x(n-j). \tag{38}$$

Now that an estimate for the error at the virtual location has been obtained, the ANC algorithms previously derived can be applied to minimize the virtual error. The performance of the ANC system is extremely dependent on the estimate of Eq. 37. It has been theoretically shown that equal amounts of attenuation of a tonal disturbance can be achieved by minimizing the estimated virtual pressure or the directly measured pressure at the virtual location, provided preliminary transfer function estimates are correct [20]. However, degradation in performance is to be expected in practice, as the preliminary identification stage will never result in perfectly accurate transfer function models.

3 Computer Simulations

Extensive computer simulations of the control structures described in Sections A-C have been performed. In a simulation environment, it is feasible to construct scenarios that showcase the benefits of each of the control structures. The following summarizes the important simulation results for different reference and disturbance signal conditions.

A System Identification

The preliminary identification stage requires three transfer functions to be modeled: the control to physical error sensor path, the control to virtual error sensor path, and the physical error sensor to virtual error sensor path. These transfer functions are obtained from an experimental ANC setup in a partially anechoic room. Very few reflections were present, therefore an FIR model adequately captures the path dynamics. The secondary paths, $G_{cp}(z)$ and $G_{cv}(z)$, are modeled as FIR filters with 150 taps. The estimates, $\hat{G}_{cp}(z)$ and $\hat{G}_{cv}(z)$, are modeled using only 75 taps as to induce an error in the model frequency responses. The remaining transfer functions, $P(z)$ and $G_{pv}(z)$, are modeled by turning off the secondary source and driving the primary noise source with identification noise. The virtual path and it's estimate, $G_{pv}(z)$ and $\hat{G}_{pv}(z)$, are modeled as FIR filters with 100 and 90 taps, respectively. The primary path is modeled as an FIR filter with 500 taps. The bandwidth over which the model is accurately identified was set to be 50-800 Hz.

B Controller Performance

In the first simulation, the controller aims to minimize the error signal directly measured at the virtual location, rather than its estimate given by Eq. 37. This serves to illustrate performance difference between the three controllers before introducing complexities associated with a virtual sensor. The disturbance consists of a broadband signal as well as two tonal components at frequencies ω_1 and ω_2. The reference signal is correlated with the broadband component and one of the

tonal components of the disturbance. This is written

$$d(n) = P(z)x(n) + v_{nb}(n), \tag{39}$$

where $P(z)$ is the path from the disturbance to the error sensor. The reference noise, $x(n)$, consists of a broadband component and a sinusoid with frequency ω_1. The quantity $v(n)$ is a sinusoid with frequency ω_2. This condition represents a scenario in which the reference sensor is unable to observe part of the narrow-band disturbance. The frequencies are chosen as ω_1=150 Hz and ω_2=225 Hz.

The simulation results are shown in Figure 4. As expected, the feedforward controller is capable of attenuating only the disturbance that is correlated with the reference. The uncorrelated narrow-band disturbance at ω_2=225 Hz is minimally reduced. The feedback controller, which makes no use of the reference signal, is capable of attenuating both narrow-band disturbances, but provides no broadband benefit. The hybrid controller outperforms both the feedforward and feedback controllers, canceling both the disturbance correlated with the reference as well as the uncorrelated narrow-band disturbance. In situations where a noise source is not easily identifiable or measurable, hybrid control structures offer significant performance advantages over the traditional feedforward and feedback approaches.

A virtual sensor is incorporated into the second simulation. The reference and disturbance signals are not changed. The virtual pressure is estimated based on the remote microphone technique outlined in Section D. When minimizing the virtual pressure, it is important to note that the update equations given by Eq. 11, Eq. 13, Eq. 30, and Eq. 31 must be modified. The correct update equations for the hybrid controller are

$$\mathbf{a}(n+1) = \mathbf{a}(n) - \alpha_1 \hat{\mathbf{x}}_v(n)\hat{e}_v(n), \tag{40}$$

$$\mathbf{c}(n+1) = \mathbf{c}(n) - \alpha_2 \hat{\mathbf{z}}_v(n)\hat{e}_v(n), \tag{41}$$

where $\hat{x}_v(n)$ is given by Eq. 38 and

$$\hat{z}_v(n) = \sum_{j=0}^{J-1} \hat{g}_{cv_j} z(n-j). \tag{42}$$

The main difference is that the gradient is now a function of the estimated virtual error and the control to virtual sensor path. For accurate path models and virtual pressure estimates, the convergence behavior of each controller with the incorporation of a virtual sensor will be similar to the behavior using a physical sensor.

The simulation results are shown in Figure 5. The overall behavior is similar to if the virtual pressure is directly minimized. As was the case in the first simulation, the feedforward controller minimizes only the disturbance correlated with the reference noise. The feedback controller achieves nearly 10 dB reduction in the narrow-band disturbances with minimal spillover. The hybrid controller again outperforms the others. Using the estimate of the virtual pressure results in significantly less attenuation of the tonal disturbances. While the tones are almost completely cancelled when minimizing the exact virtual pressure, $e_v(n)$, only a 10-15 dB reduction is achieved when minimizing the estimate, $\hat{e}_v(n)$. This is mainly due to modeling errors on the secondary path transfer functions. If perfect transfer function models are assumed, the attenuation levels obtained by minimizing $e_v(n)$ and $\hat{e}_v(n)$ are comparable.

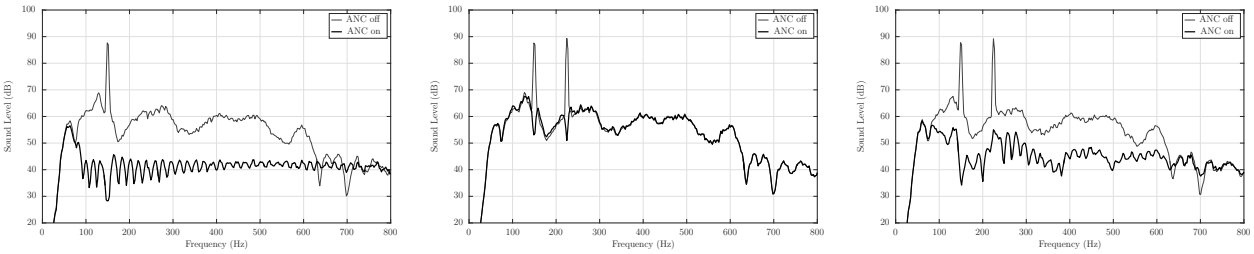

(a) Feedforward controller performance.

(b) Feedback controller performance.

(c) Hybrid controller performance.

Figure 4: Simulation results for feedforward, feedback, and hybrid control structures. The reference signal consists of a 150 Hz tone and a broadband signal. The disturbance is the reference signal filtered through $P(z)$ plus an uncorrelated sinusoid of frequency 225 Hz.

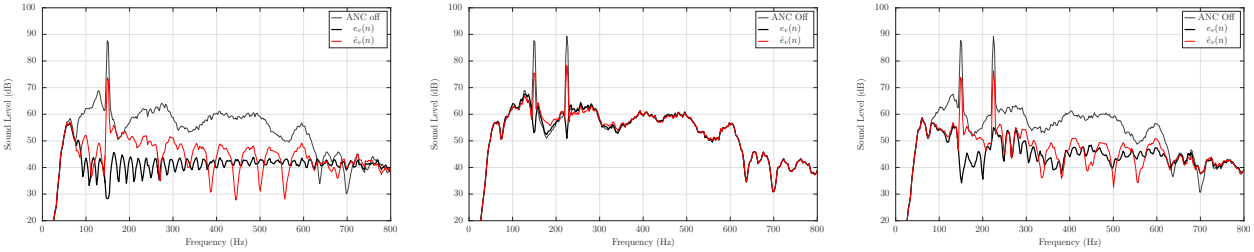

(a) Feedforward controller performance.

(b) Feedback controller performance.

(c) Hybrid controller performance.

Figure 5: Simulation results for feedforward, feedback, and hybrid control structures. Shown are the spectra obtained from directly minimizing the virtual pressure and minimizing the estimate. The reference signal consists of a 150 Hz tone and a broadband signal. The disturbance is the reference signal filtered through $P(z)$ plus an uncorrelated sinusoid of frequency 225 Hz.

4 Control Experiments

A single channel ANC experiment was carried out in a partially anechoic room. The reference microphone was placed adjacent to the disturbance source and roughly 2 m from the error sensor. This ensures that the reference sensor is providing time advanced information to the controller. Each of the scenarios described in the simulations were created. Simulink models of each control structure were built. The platform used to interface to the speakers, microphones, and host computer is an XPC Target computer. This machine is used with Simulink Real-Time to compile Simulink models, download them to the target machine, and run them in real time.

It has been clearly demonstrated that an advantage of the hybrid controller is its ability to attenuate uncorrelated narrow-band disturbances while maintaining the performance advantages of feedforward control. This scenario is easy to devise in a simulation environment, but has not received much attention in ANC experiments. This is mainly because in laboratory experiments, the reference sensors are judiciously placed as to observe all of the disturbance components.

In these experiments, a novel method of creating disturbances described by Eq. 39 is devised. This results in correlated broadband and narrow-band disturbances as well as uncorrelated narrow-band disturbances. The uncorrelated disturbance is created by passing the reference signal through a notch filter with notch frequency ω_n. The notch frequency is set equal to the tonal disturbance

frequency ω_2=225 Hz. This results in a reference signal used by the controller that is coherent with the disturbance everywhere except ω_n.

Before operation of the ANC system, all secondary paths must be modeled in a preliminary identification stage. The secondary paths $G_{cp}(z)$ and $G_{cv}(z)$ are each modeled as FIR filters with 400 coefficients. The virtual path $G_{pv}(z)$ is modeled as an FIR filter with 300 coefficients. Although the sensors at the virtual locations are not used during operation of the ANC system, they remain in place to monitor control performance. In the first experiment, the controller aims to minimize the pressure directly measured at the physical error sensor. This is the standard approach taken by most ANC systems. The results are shown in Figure 6. These results confirm the simulation results from Figure 4. The feedforward controller attenuates all disturbances correlated with the reference. Only control of tonal disturbances is achieved by the feedback controller. The hybrid controller shows a reduction in both narrow-band and broadband disturbance components.

The next experiment aims to minimize the pressure at the virtual error sensor location. The virtual microphone is located 10 cm from the physical microphone. The estimate is calculated according to 37. A microphone at the virtual location is used to measure the true virtual pressure. Results are shown in Figure 7. Less attenuation is achieved over the disturbance bandwidth when using a virtual sensor. This may be attributed to inaccuracies in secondary path modeling. The hybrid controller again outperforms the feedforward and feedback controllers. The tonal disturbances are attenuated by 15-20 dB and the broadband disturbances are reduced by 10-15 dB.

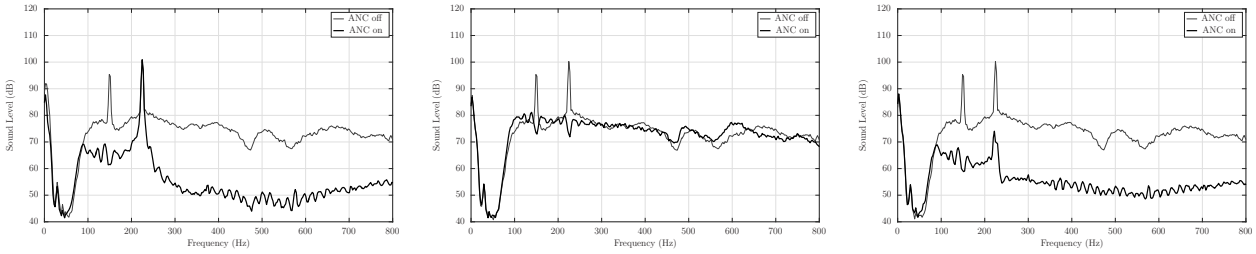

(a) Feedforward controller performance.

(b) Feedback controller performance.

(c) Hybrid controller performance.

Figure 6: Experimental results of minimizing the pressure directly at the physical error sensor. The reference signal consists of a 150 Hz tone and a broadband signal. The disturbance is the reference signal filtered through $P(z)$ plus an uncorrelated sinusoid of frequency 225 Hz.

5 Conclusions

Performance characteristics of adaptive feedforward, feedback, and hybrid ANC systems have been discussed. Experiments have been carried out to characterize the performance of each controller. Feedforward control is capable of attenuating disturbance components that are correlated with the feedforward reference signal. Feedback control is capable of attenuating narrow-band disturbances. A hybrid controller was also presented that outperforms both the feedforward and feedback controllers. It was shown that 15-20 dB reduction in broadband disturbances can be achieved with a hybrid controller.

A method for estimating pressure at remote locations has also been presented. The incorporation of a virtual sensor into ANC systems was also discussed. Simulation and experimental results have shown that it is feasible to create quiet zones at these virtual locations. Experimental results

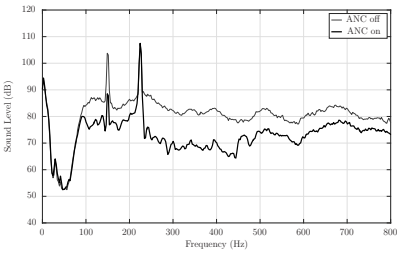

(a) Feedforward controller performance.

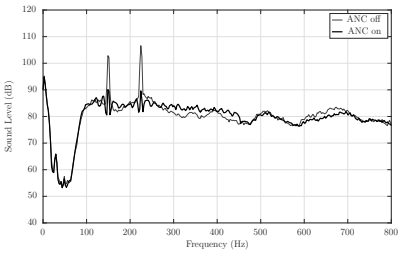

(b) Feedback controller performance.

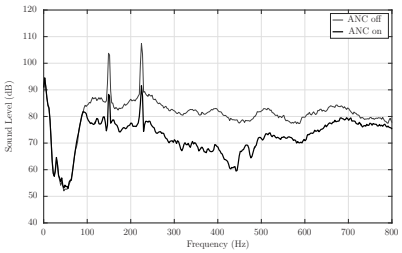

(c) Hybrid controller performance.

Figure 7: Experimental results of minimizing the estimated pressure at the virtual location. The reference signal consists of a 150 Hz tone and a broadband signal. The disturbance is the reference signal filtered through $P(z)$ plus an uncorrelated sinusoid of frequency 225 Hz.

show a 10-15 dB reduction in broadband disturbances at the virtual location when using the hybrid controller. With accurate secondary path models, attenuation levels comparable to those obtained by minimizing pressure directly at a physical microphone can be achieved at virtual locations.

REFERENCES

[1] Paul Lueg. Process of silencing sound oscillations, June 1936.

[2] S.J. Elliot and P.A. Nelson. Active Noise Control. *Signal Processing Magazine, IEEE*, 10(4):12–35, 1993.

[3] S.M. Kuo and D.R. Morgan. Active noise control: a tutorial review. In *Proceedings of the IEEE*, volume 87, pages 943–973, 1999.

[4] P.A. Nelson and S.J. Elliott. *Active control of sound*. Academic Press, 1993.

[5] M.R. Bai and H.H. Lin. Comparison of Active Noise Control Structures in the Presence of Acoustical Feedback by using the H$_{\infty}$ Synthesis Technique. *Journal of Sound and Vibration*, 206(4):453–471, 1997.

[6] C. Bao, R. Paurobally, and J. Pan. Design and test of a Feedback Controller for Attenuating Low Frequency Noise in a Room. *Acoustics Australia*, 37(2):61–66, 2009.

[7] A.J. Hull, C.J. Radcliffe, and S.C. Southward. Global Active Noise Control of a One-Dimensional Acoustic Duct using a Feedback Controller. *Transactions of ASME*, 115:488–494, 1993.

[8] B. Widrow and S. Stearns. *Adaptive Signal Processing*. Prentice Hall, 1985.

[9] S.J. Elliot. *Signal Processing for Active Control*. Academic Press, 2001.

[10] J Garcia-Bonito, S.J. Elliot, and C.C. Boucher. Generation of zones of quiet using a virtual microphone arrangement. *Journal of the Acoustical Society of America*, 101(6):3489–3516, 1997.

[11] B. Rafaely, S.J. Elliot, and J Garcia-Bonito. Broadband performance of an active headrest. *Journal of the Acoustical Society of America*, 106(2):787–793, 1999.

[12] Marek Pawelczyk. Adaptive noise control algorithms for active headrest system. *Control Engineering Practice*, 12:1101–1112, 2004.

[13] Marek Pawelczyk. Multiple input multiple output adaptive feedback control strategies for the active headrest system: design and real-time implementation. *INTERNATIONAL JOURNAL OF ADAPTIVE CONTROL AND SIGNAL PROCESSING*, 17:785–800, 2003.

[14] X. Kong, Pu Liu, and S.M. Kuo. Multiple channel hybrid active noise control systems. *IEEE Transactions on Control Systems Technology*, 6(6):719–729, 1998.

[15] A. Roure and A. Albarrazin. The remote microphone technique for active noise control. In *Active 99'*, pages 1233–1244, Florida, USA, 2000.

[16] S.J. Elliot, I.M. Stothers, and P.A. Nelson. A Multiple Error LMS Algorithm and Its Application to the Active Control of Sound and Vibration. *IEEE Transactions on Acoustics, Speech, and Signal Processing*, 35(10):1423–1434, 1987.

[17] G.C. Newton, L.A. Gould, and J.F. Kaiser. *Analytical Design of Linear Feedback Controls*. Wiley, 1957.

[18] B. Rafaely and S. Elliot. Adaptive Internal Model Controller-Stability Analysis. In *Internoise*, pages 983–988, 1996.

[19] M. Vaudrey, W. Baumann, and W. Saunders. Stability and operatingconstraints of adaptive LMS-based feedback control. *Automatica*, 39:595–605, 2003.

[20] C.J. Radcliffe and S. Gogate. A model based feedforward noise control algorithm for vehicle interiors. In *Advanced Automotive Technologies ASME*, volume 52.